2009

X-RAY AND ULTRAVIOLET SPECTROSCOPY OF GALACTIC DIFFUSE HOT GAS ALONG THE LARGE MAGELLANIC CLOUD X-3 SIGHT LINE

Y Yao

QD Wang
University of Massachusetts - Amherst, wqd@astro.umass.edu

T Hagihara

K Mitsuda

D McCammon

See next page for additional authors

Authors
Y Yao, QD Wang, T Hagihara, K Mitsuda, D McCammon, and NY Yamasaki

Accepted for publication in the Astrophysical Journal
Preprint typeset using LaTeX style emulateapj v. 10/09/06

X-RAY AND UV SPECTROSCOPY OF GALACTIC DIFFUSE HOT GAS ALONG THE LMC X–3 SIGHT LINE

Y. Yao[1,2], Q. D. Wang[3], T. Hagihara[4], K. Mitsuda[4], D. McCammon[5], and N. Y. Yamasaki[4]
Accepted for publication in the Astrophysical Journal

ABSTRACT

We present *Suzaku* spectra of X-ray emission in the fields just off the LMC X–3 sight line. O VII, O VIII, and Ne IX emission lines are clearly detected, suggesting the presence of an optically thin thermal plasma with an average temperature of 2.4×10^6 K. This temperature is significantly higher than that inferred from existing X-ray absorption line data obtained with *Chandra* grating observations of LMC X–3, strongly suggesting that the gas is not isothermal. We then jointly analyze these data to characterize the spatial and temperature distributions of the gas. Assuming a vertical exponential Galactic disk model, we estimate the gas temperature and density at the Galactic plane and their scale heights as $3.6(2.9,4.7)\times 10^6$ K and $1.4(0.3,3.4)\times 10^{-3}$ cm^{-3} and $1.4(0.2,5.2)$ kpc and $2.8(1.0,6.4)$ kpc, respectively. This characterization can account for all the O VI line absorption, as observed in a *FUSE* spectrum of LMC X–3, but only predicts less than one tenth of the O VI line emission intensity typically detected at high Galactic latitudes. The bulk of the O VI emission most likely arises at interfaces between cool and hot gases.

Subject headings: X-rays: diffuse background – Galaxy: halo — X-rays: ISM

1. INTRODUCTION

The Galactic diffuse hot gas at temperatures $\sim 10^6$ K can be effectively probed via its emission and absorption features in X-ray and far-ultraviolet (UV) wavelength bands. The previous X-ray emission investigations were largely based on the broadband X-ray background data, e.g., *ROSAT ALL Sky Survey* (RASS; Snowden et al. 1997). A high spectral resolution X-ray calorimeter abroad a sounding rocket, though providing little spatial resolution, clearly detected the O VII and O VIII emission lines, confirming that much of the soft X-ray background (SXB) emission is thermal in origin (McCammon et al. 2002). Recently, several groups have attempted to study the background emission with X-ray CCDs aboard *Suzaku X-ray Observatory*, which, compared to those on *XMM-Newton* and *Chandra X-ray observatories*, have a significantly improved spectral resolution and a low instrument background (e.g., Smith et al. 2007; Henley & Shelton 2007). These later X-ray observatories, however, also carry the high resolution grating instruments that allow for the detection of the X-ray absorption lines (e.g., from O VII, O VIII, and Ne IX Kα transitions) by diffuse hot gas in and around the Galaxy. Indeed, such absorption lines are detected in grating spectra of nearly all Galactic and extragalactic sources as long as the spectral signal-to-noise ratio is high enough (e.g., Futamoto et al. 2004; Yao & Wang 2005; Fang et al. 2006; Bregman & Llyoid-Davis 2007). These X-ray absorption lines trace gas over a broad temperature range of $\sim 10^{5.5}-10^{6.5}$ K.

Gas at temperatures $\lesssim 10^{5.5}$ K may be traced more sensitively in far-UV, via the detection of the O VI lines at $\lambda\lambda$1031.96 and 1037.62. Extensive observations of the lines in absorption have been carried out with *Copernicus* and *Far Ultraviolet Spectroscopy Explorer* (*FUSE*; Jenkins 1978; Savage et al. 2003; Bowen et al. 2008). In addition, the O VI lines have also been detected in emission with *FUSE*, although the sky is only sampled at various Galactic latitudes (e.g., Shelton et al. 2001; Otte & Dixon 2006). The intensity of the λ1031.96 line, for example, ranges from 1800 to 9100 LU (line unit; 1 photon cm^{-2} s^{-1} sr^{-1}). However, the interpretation of the O VI line(s) alone is not straight forward, because in the collisional ionization equilibrium (CIE) state, the O VI population sharply peaks at the intermediate temperature $\sim 10^{5.5}$ K where gas cools very efficiently (Sutherland & Dopita 1993). Thus such O VI-bearing gas is expected to be rare and may preferentially reside at interfaces between cool gas clouds and thermally more stable hot gas. But this latter hot gas, which should be more abundant, distributed more widely, and effectively traced by the X-ray O VII line, could contribute significantly to the O VI line as well. Currently, little is known about the relative contributions from these two origins to the O VI, either in absorption or in emission.

Clearly, a combined analysis of the X-ray and far-UV lines, in both emission and absorption, will be the most beneficial. While an absorption line is proportional to the total column density of the gas integrated along a line of sight, an emission line depends on the emission measure (EM) of the gas. Furthermore, for a gas in the CIE state, both the ionic column density and the EM depend on the gas temperature, but in different manners (Fig. 1). Therefore a joint analysis of multiple emission/absorption lines will enable us to constrain not only the temperature and its distribution but also the size and density of the intervening gas (e.g., Shull & Slavin 1994). When transitions from multiple elements (e.g., O and Ne) are detected, their relative abundances can also be estimated (Yao & Wang 2006). Such a joint analysis has been tentatively applied to several sources (e.g., Yao & Wang 2007; Shelton et al. 2007); but none of these sources has high resolution emission and absorption data available in both X-ray and far-UV wavelength bands.

In this paper, we report our investigation of the hot gas along the sight line toward LMC X–3. Wang et al. (2005)

[1] Massachusetts Institute of Technology (MIT) Kavli Institute for Astrophysics and Space Research, 70 Vassar Street, Cambridge, MA 02139; yaoys@space.mit.edu
[2] University of Colorado, CASA, 389 UCB, Boulder, CO 80309; yaoys@colorado.edu
[3] Department of Astronomy, University of Massachusetts, Amherst, MA 01003
[4] Department of High Energy Astrophysics, Institute of Space and Astronautical Science (ISAS), Japan Aerospace Exploration Agency (JAXA), 3-1-1, Yoshinodai, Sagamihara, 229-8510, Japan
[5] Department of Physics, University of Wisconsin-Madison, 1150 University Avenue, Madison, WI 53706

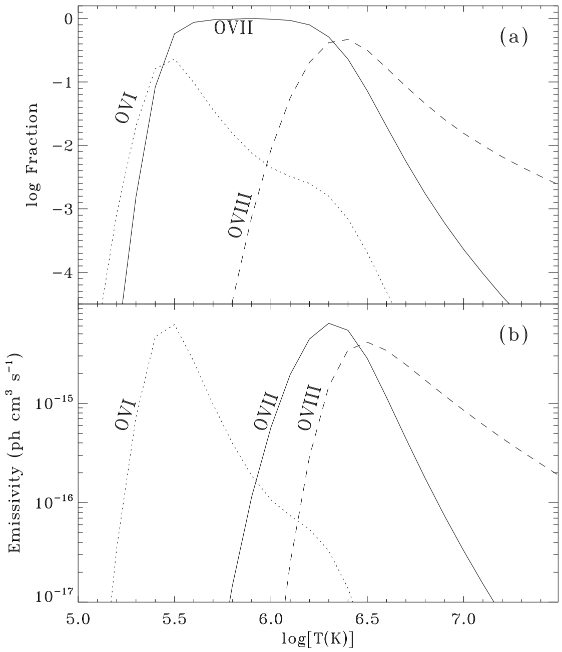

FIG. 1.— Ionization fraction (a) and the emissivity (b) of oxygen ions as a function of temperature for a gas in the collisional ionization equilibrium state (Sutherland & Dopita 1993). The emissivity is a summation of the doublet transitions at 1031.96 Å and 1037.62 Å (O VI), triplet transitions at 22.10 Å, 21.80 Å, and 21.60 Å (O VII), and Kα plus Kβ transitions at 18.97 Å and 16.0 Å (O VIII). The emissivity of O VI is scaled down by a factor of 1000 for demonstration purpose.

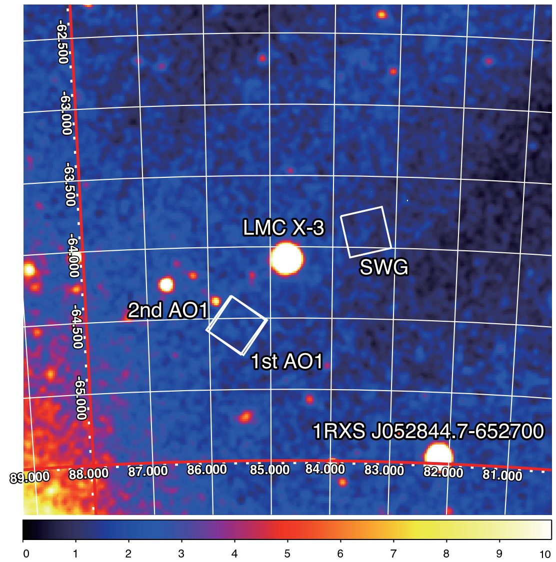

FIG. 2.— *RASS* 0.1-2keV band X-ray map in the vicinity of LMC X-3 (the bright source at the center) and the XIS field of view of the three presented observations.

have reported the detection of the hot gas associated with our Galaxy, based on X-ray and far-UV absorption line spectra from *Chandra* and *FUSE* observations. Here we present the *Suzaku* CCD emission spectra of the X-ray background in two fields adjacent to the LMC X–3 sight line. This unique combination of the X-ray and far-UV spectral data toward essentially the same part of the sky further allows us to constrain the spatial, thermal, and chemical properties of the hot gas.

This paper is organized as follows. We present the *Suzaku* observations and the data calibration, as well as a brief description of the existing *Chandra* and *FUSE* data in § 2. In § 3, we first analyze the X-ray emission (§ 3.1) and absorption (§ 3.2) data separately, and then build a slab-like hot gas model to jointly analyze these X-ray data (§ 3.3). In § 3.4, we compare the model predicted O VI absorptions with the *FUSE* detections, and then use the observed O VI absorption line to further constrain our model. We discuss the implications of our results in § 4 and summarize our results and conclusions in § 5.

Throughout the paper, we assume the hot emitting/absorbing gas to be optically thin (see § 4.3 for further discussion) and in the CIE state. We adopt the solar abundances from Anders & Grevesse (1989) and quote parameter errors at 90% confidence levels for a single varying parameter unless otherwise noted. We also refer the hot gas on scales of several kpc as the Galactic disk, in contrast to the Galactic halo on scales of > 10 kpc (see § 4.4 for further discussion). Our spectral analysis uses the software package XSPEC (version 11.3.2).

2. OBSERVATIONS AND DATA REDUCTION

2.1. *Suzaku observations*

We observed the emission of the hot diffuse gas toward off-fields of the LMC X–3 sight line once during the science working group (SWG) program and twice during the AO1 program (Table 1), using the CCD camera XIS (Koyama et al. 2007) on board *Suzaku* (Mitsuda et al. 2007). To obtain the diffuse gas emission as close as to the LMC X–3 sight line along which the X-ray O VII absorption line has been detected (see § 2.2) but with a minimized confusion by stray lights from the point source, and to average out the possible spatial gradient of the diffuse emission intensity, we observed two fields that are in nearly opposite directions from LMC X–3 and $\sim 30'$ away from it, as illustrated in Figure 2. With this configuration and the roll angle of the XIS field of view, we estimate that stray lights from LMC X–3 contribute no more than 6% to the observed X-ray emission in 0.3–1.0 keV energy range during our observations. The XIS was set to the normal clocking mode and the data format was either 3×3 or 5×5, and the spaced-raw charge injection (SCI) was not applied to any of the data during the observations.

We used processed data version 1.0.1.1 for the SWG observation and version 2.0.6.13 for the two AO1 observations. We adopted the standard data selection criteria to obtain the good time intervals (GTIs), i.e., excluding exposures when the *Suzaku*'s line of sight is elevated above the Earth rim by less than 10° and exposures with the "cut-off rigidity" less than 6 GV (please refer to Smith et al. 2007 for further information). We checked the column density of the Sun-lit atmosphere during the selected GTIs, and found that it is always below 1.0×10^{15} cm^{-2}, which is the criterion for no significant neutral oxygen emission from the Earth's atmosphere (Smith et al. 2007). We also converted the pulse-height-analysis (PHA) channels of X-ray events to pulse-invariant (PI) ones by using the *xispi* script (version 2006-5-16 for SWG and version 2007-05-30 for AO1 observations).

We created X-ray images in 0.3–2.0 keV energy range for the three observations, and found three discrete X-ray sources in the SWG data. To obtain the "true" diffuse emission, we removed those events within circular regions centered at the sources with a radius of $1'$ for the two faint sources and $3'$ for the bright one. Modeling these discrete sources we estimated the contamination of their stray lines to the diffuse emission to be less than 5% in 0.3–2.0 keV energy band.

TABLE 1
Suzaku OBSERVATION LOG

	SWG	1st AO1	2nd AO1
Aim point [a] (J2000)	(83.4720,-63.9000)	(85.5500,-64.5500)	(85.5500,-64.5500)
Observation start times (UT)	14:06:44, 17 March 2006	03:27:42, 22 April 2006	07:35:00, 31 October 2006
Observation end times (UT)	21:48:52, 19 March 2006	00:14:19, 23 April, 2006	18:01:24, 31 October 2006
Exposure time	80 ks	50 ks	compensation for 1st AO1
Exposure after data selection	83.9 ks	22.5 ks	14.5 ks

NOTE. — [a] Aim point on the focal plane is the XIS nominal position.

In the last step, we excluded those events severely affected by the solar activity. The diffuse X-ray emission below 1 keV could be contaminated by X-ray emission of the solar wind charge exchange (SWCX) if the proton flux exceeds 3×10^{8} s^{-1}cm^{-2} in the wind (Mitsuda et al. 2008). The probability of such contamination increases if the shortest Earth-to-magnetopause (ETM) distance is $\lesssim$10 Earth radius ($R_{\rm E}$) (Fujimoto et al. 2007). Here, the magnetopause is defined as the lowest position along the line of sight where geomagnetic field is open to interplanetary space. We used solar wind data obtained with the Solar Wind Electron, Proton, and Alpha Monitor (SWEPAM) aboard the *Advanced Composition Explorer* (*ACE*) [6]. We found that there are some time intervals with proton flux exceeding the above limit during the SWG and the first AO1 observations. We thus sub-divided the observations and constructed X-ray spectra for various flux levels, and found that, for the SWG observation, the spectra are consistent with each other, while for the first AO1 observation the O VII and O VIII intensities are enhanced in the high flux subsets. We then calculated the ETM distance, and found that during the SWG observation, it is always longer than 5 $R_{\rm E}$ when the magnetic field is open to the Sun direction and that it becomes as short as 1.4 $R_{\rm E}$ when the magnetic field is open to anti-Sun direction during which however solar-wind particles cannot penetrate. In contrast, during the first AO1 observation the ETM distance varies significantly and some times becomes shorter than 3 $R_{\rm E}$ even when the magnetic field is open to the Sun direction. We further sorted the first AO1 data according to this distance and the solar wind flux, and decided to use only those time intervals with the proton flux $< 3\times10^{8}$ s^{-1}cm^{-2} or the ETM distance $> 3R_{\rm E}$, during which spectra of the SWG and the AO1 data are all consistent.

We estimated the non-X-ray background from the night Earth database using the method described in Tawa et al. (2008). We found that for XIS1, the count rate discrepancy between the database and our observations is about 5% above 10 keV, which indicates the background uncertain level. Since the non-X-ray background is only 10% of the diffuse emission for the energies below 1 keV, this uncertainty is negligible.

We constructed instrumental response files (rmf) and effective area (arf) by running the scripts *xisrmfgen* and *xissimarfgen* (version 2006-10-26; Ishisaki et al. 2007). To take into account of the diffuse stray light effects, we used a 20′-radius flat field as the input emission in calculating the arf. We also included in the arf file the degradation of low energy efficiency due to the contamination on the XIS optical blocking filter.

In this work, we only used the spectra obtained with XIS1, which is a backside-illuminated CCD chip and is of high sensitivity at photon energies below 2 keV compared to the other three frontside-illuminated CCDs, XIS0 and XIS2-3 (Koyama et al. 2007). We grouped the spectra to a signal-to-noise ratio of ≥ 10 in each channel, and used energy range of 0.4-3.0 keV in our analysis. This range is broad enough for constraining the continuum and also covers the H- and He-like emission lines of nitrogen, oxygen, neon, magnesium, and L transition of Fe XVII. The N VII, O VII, O VIII, and Ne IX lines are clearly visible in the spectra (Fig. 3).

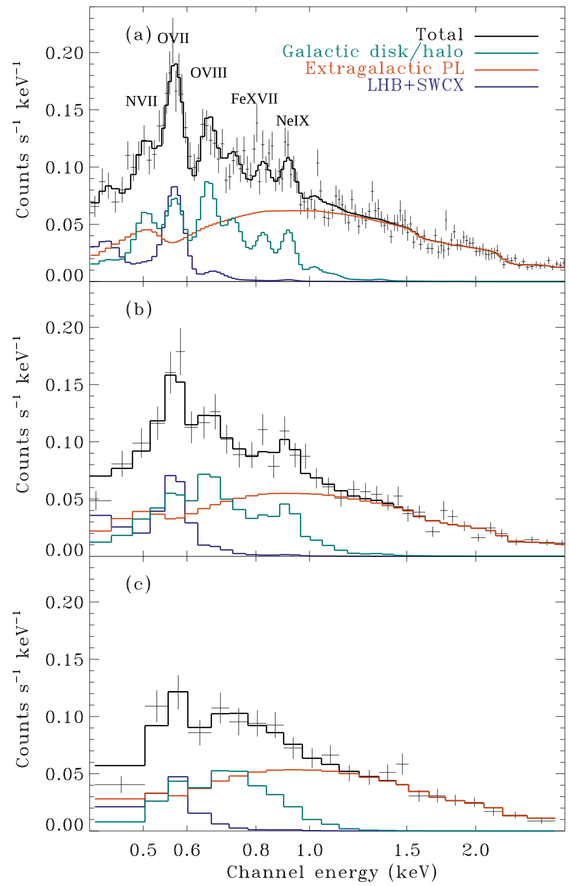

FIG. 3.— The background emission spectra in the off-fields of the LMC X–3 sight line obtained with *Suzaku* XIS1 in the SWG (*a*), the first AO1 (*b*), and the second AO1 (*c*) observations, respectively. The spectra were re-grouped to be with a signal-to-noise ratio of ≥ 10.

The observed diffuse X-ray emission is mainly from the Galactic gas and confusion from the LMC is little. The targeted sight lines are well outside the main body of the LMC and is $\sim 5^{\circ}$ away from the active star-forming 30 Doradus region (see Fig. 1 in Wang et al. 2005). Toward these sight lines, there is no evidence for the present of a large-scale halo; the hot halo gas producing the observed O VII and O VIII emission could be at too high temperatures to be confined by the LMC. Furthermore, comparing to the AO1 pointings, the SWG pointing is $\sim 1^{\circ}$ degree further away from the LMC (Fig. 2). The consistent measurements between the observa-

[6] See http://www.srl.caltech.edu/ACE/ASC/level2.

TABLE 2
LINE MEASUREMENTS

	O VI	O VII	O VIII	Ne IX	N VII
EW (mÅ)[a]	235.8 ± 37.5	20 ± 6	< 4.1	6.3 ± 2.6	< 1.7
I (LU)[b]	···	5.0 ± 0.8	2.5 ± 0.4	1.0 ± 0.2	2.9 ± 2.0

NOTE. — [a] Equivalent width of the absorption lines reported in Wang et al. (2005), except for N VII that is measured in this work. [b] Line intensity (1 LU = 1 photon cm^{-2} s^{-1} sr^{-1}) measured from the unresolved triplet of O VII and Ne IX, and Kα of O VIII and N VII in § 3.1.

tions (see § 3.1) indicate a lack of a radial gradient that could be expected in any LMC emission contribution. We therefore conclude that the LMC contribution to the observed emission, if any, is negligible.

2.2. *Chandra and FUSE observations*

Chandra and *FUSE* observed LMC X–3 with exposures of $\sim$ 100 and 120 ks, respectively. Based on these observations, Wang et al. (2005) reported the detection of O VII, Ne IX, and O VI absorption lines along the sight line. For ease of reference, we list these detection in Table 2. A joint analysis of the detected O VII and Ne IX Kα absorption lines, together with the non-detection lines of O VII Kβ and O VIII Kα, allowed for the measurements of the characteristic temperature, velocity dispersion, and oxygen column density of hot gas along the sight line with little confusion with extragalactic gas (Wang et al. 2005). We adopted the same co-added spectra and the corresponding calibration files as obtained in Wang et al. (2005). Because the *Chandra* observation was carried out with the high resolution camera (HRC) that has very little energy resolution itself, the spectrum therefore needs to be fitted in a broad spectral range with an order-combined response file in order to take into account the grating-order overlapping (please refer to Wang et al. 2005). To easily implement, we further extracted the first grating order spectrum by doing the following. We first obtained a "global" best fit to the spectrum over the wavelength range of 2-30 Å, and then subtracted the spectrum channel by channel by the difference of the model-predicted counts between based on the order-combined response file and based on the first-order response file. We used the first-order spectrum in ranges of 12-22, and 24-29.5 Å, covering the L transition of the Fe XVII as well as the K transitions of the H- and He-like neon, oxygen, and nitrogen ions. To facilitate a joint analysis of the X-ray absorption and emission spectra with the O VI absorption line measurement, we re-wrote the *FUSE* spectral file produced with the CALFUSE pipeline in a format that can be read into the XSPEC. A Gaussian profile with a full-width-half-maximum of 20 km s^{-1} was used to mimic the instrumental response of the *FUSE* data.

Wang et al. (2005) argued that the observed absorption lines trace the Galactic gas rather than any intrinsic material associated with LMC X–3. Here we recapitulate their argument in the following. LMC X–3 has a systematic velocity of $\sim$ 300 km s^{-1}. However, with the typical velocity resolution of $\sim$ 20 km s^{-1} offered by *FUSE*, the centroid of the O VI absorption line was measured as 55 ± 11 km s^{-1} (1σ error), which is > 10 σ smaller than the velocity of LMC X–3. The consistent measurements of this line in two observations with different source flux also indicate a Galactic origin. In measuring the absolute wavelength, current X-ray instruments can not offer a significantly better resolution than that systematic velocity, but *Chandra* grating observations can provide a relative wavelength measurement as accurate as several tens kilometer per second. Wang et al. found that the velocity shifts of the O VII, the low ionization O I Kα lines, and the wavelength interval between these two lines are consistent with those observed toward a Galactic source 4U 1820–303 and two extragalactic sources Mrk 421 and PKS 2155–304; the lines along the latter three sight lines are believed to have a Galactic origin. On the other hand, if the absorptions are associated with the LMC X–3 as in a photo-ionized wind scenario, the line width and velocity shift are expected to be on the order of the escaping velocity of the system ($\sim 10^3$ km s^{-1}), which is inconsistent with the narrowness and rest-frame velocity of the observed O VII and O VI lines. They then attributed the observed absorptions to the Galactic gas, which is also assumed in this work.

In the *FUSE* spectra of LMC X–3, Hutchings et al. (2003) and Wang et al. (2005) also found an O VI emission line whose velocity centroid varies as a function of the binary phase. This phase dependency could be explained if the emission arises from the companion star illuminated by the X-ray primary (L. Song et al. in preparation). The similar X-ray O VII emission has not been observed. The lines of our interests in this work are all very narrow (with a FWHM of $\sim 10^2$ km s^{-1}) and their measurements depend on the local continuum. The observed emission line is very broad (with a half-width of $\sim 10^3$ km s^{-1}) and therefore will not affect our measurements herein presented.

3. ANALYSIS AND RESULTS

3.1. *Fit to X-ray emission data*

The SXB emission is a composite of various components. Chiefly among them are the diffuse hot gas associated with the large-scale Galactic disk/halo, the Local Hot Bubble (LHB), the SWCX, and the extragalactic (primarily from unresolved AGNs) and the Galactic (mainly unresolved stars) discrete sources. Recent X-ray shadowing experiments with *Suzaku* and *XMM-Newton* indicate that the combined contribution from the LHB and the SWCX can be described with an emitting plasma at a temperature of $\sim 1.2 \times 10^6$ K with an EM of 0.0075 cm^{-6} pc (Smith et al. 2007; Galeazzi et al. 2007; Henley et al. 2007), which is equivalent to the line intensities of 3.5 and 0.04 LU for O VII triplet and O VIII, respectively. The contribution from unresolved stellar sources is expected to be negligible at high galactic latitudes ($|b| > 30°$; Kuntz & Snowden 2001) and is not further considered in this work. The extragalactic emission contribution can be approximated as a power-law (PL) with an index of $\sim$ 1.4 and a normalization of $\sim$ 10.9 photons cm^{-2} kev^{-1} s^{-1} sr^{-1} at 1 keV (e.g., Hickox & Markevitch 2006; see § 4.2 for further discussion).

We decompose the SXB emission in the LMC X–3 off-fields by jointly fitting the three *Suzaku* emission spectra. We first fit the spectra with an XSPEC model combination of $\mathrm{mekal_{LHB}}$ + wabs($\mathrm{powerlaw_{exg}}$ + $\mathrm{vmekal_{disk}}$). We fix the cool gas absorption (wabs) to be $N_H^c = 3.8 \times 10^{20}$ cm^{-2}, derived from the neutral absorption edge study (Page et al. 2003). We assume the Galactic diffuse hot gas (as denoted by $\mathrm{vmekal_{disk}}$) to be isothermal, let the abundances of nitrogen, neon, and iron to be fitting parameters, and fix the abundance ratios between other metal elements and oxygen to the solar values. We also fix the LHB component to the values mentioned above (but see § 4.1 for further discussion) and allow the normalization of the extragalactic PL component ($\mathrm{powerlaw_{exg}}$) to vary in the fit (accounting for the cosmic variance). This simple model combination fits the emission data well. The

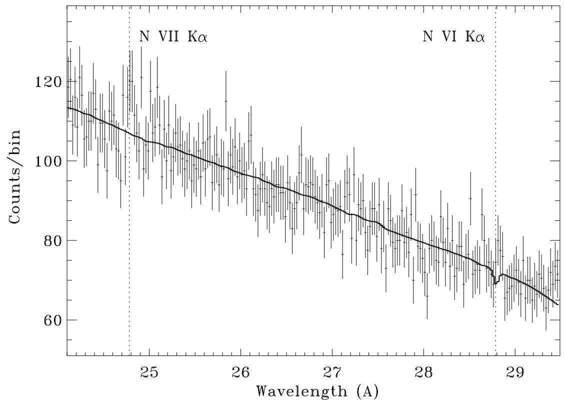

FIG. 4.— The *Chandra* count spectrum around N VI and N VII Kα absorption lines. The dotted lines mark the rest-frame wavelength positions. The solid line represents the best-fit continuum and the predicted absorptions, assuming the solar value of N/O. The binsize is 25 mÅ.

fitting parameters are consistent among the three observations except for slightly higher nitrogen abundance and PL normalization values for the SWG data. The discrepancy in the nitrogen abundance is probably due to the calibration uncertainty of the XIS1 for the SWG observation taken at early stage (see § 3.2), while the high PL normalization is likely caused by the residual contamination (the wing of the point spread function) of the relatively bright field source that cannot be completely excluded from the SWG data (§ 2.1). We then link all fitting parameters among three observations except for nitrogen abundance, the PL index, and PL normalization, which are linked within the two AO1 observations but are allowed to vary between AO1 and SWG ones. The fit is acceptable with $\chi^2/dof = 194/179$ (Fig. 3). The fitting parameters are presented in the first row of Table 3. By setting the abundances of nitrogen, oxygen, and neon in the Galactic disk component to be zero, and using Gaussian profiles to fit the N VII, O VII, O VIII and Ne IX lines at 0.50, 0.56, 0.65, and 0.91 keV, we measure the intrinsic (cool-gas-absorption corrected) emission line intensities of the diffuse hot gas (Table 2).

3.2. *Fit to X-ray absorption data*

Assuming the intervening gas to be isothermal and adopting the ISM metal abundances from Wilms et al. (2000), Wang et al. (2005) constrained the gas temperature, velocity dispersion, and O VII (or equivalent hydrogen) column density, by jointly analyzing the detected O VII and Ne IX Kα absorption lines with the non-detections of O VII Kβ and O VIII Kα lines. Following the same procedure, we have re-fitted the spectrum reduced in § 2.2 and obtained nearly identical results to those obtained by Wang et al. (the second row in Table 3), except for the equivalent hydrogen column density N_H due to the different oxygen abundance adopted here. In order to compare with the *Suzaku* result on the relative abundance of N/O, we further included the non-detected N VI and N VII Kα absorption lines in our fit (Fig. 4; Table 2). The fit gives a 95% upper limit, N/O$<$2.2, which is consistent with the value constrained from the *Suzaku* AO1 data, but is lower than that inferred from the SWG data. We therefore attribute the apparent super-solar nitrogen abundance observed in the SWG data to the instrumental calibration uncertainty.

From now on, we let the normalization of the extragalactic PL component and the N/O ratio for the SWG observation vary independently from those for the AO ones in our data analysis. We will not further discuss these values in the text but still list them in our resulting Table 3 for references.

The gas temperature inferred from the above absorption line fits is a factor of ~ 2 lower than that constrained from the emission spectral analysis (§ 3.1; Table 3). We note that the temperature would be even lower if a super-solar Ne/O value as indicated in the emission spectral analysis (§ 3.1) were adopted in our absorption line fits. This temperature inconsistency clearly indicates that the X-ray emitting/absorbing gas is not isothermal. In this case, the emission and absorption arise preferentially in different temperature ranges.

3.3. *Non-isothermal model and joint fit*

Motivated by the observed morphology of diffuse X-ray emission around the nearby disk galaxies, Yao & Wang (2007) constructed a non-isothermal model for the Galactic disk hot gas. In the following, we first briefly formulize this model and then constrain it using the obtained absorption and emission data along the LMC X–3 sight line.

Assuming that the hydrogen number density and temperature of the hot gas can be characterized as

$$n = n_0 e^{-z/(h_{\rm n}\xi)} \text{ and } T = T_0 e^{-z/(h_{\rm T}\xi)}, \qquad (1)$$

where z is the vertical distance away from the Galactic plane, n_0 and T_0 are the mid-plane values, and $h_{\rm n}$ and $h_{\rm T}$ are the scale heights, and ξ is the volume filling factor that is assumed to be 1 in the paper, we can derive

$$n = n_0 (T/T_0)^{\gamma}, \qquad (2)$$

where $\gamma = h_{\rm T}/h_{\rm n}$. Therefore, the differential hydrogen column density distribution is also a power law function of T,

$$dN_H = ndL = \frac{N_{\rm H}\gamma}{T_0}(T/T_0)^{\gamma-1}dT, \qquad (3)$$

and the corresponding ionic column density along a sight line with a Galactic latitude b can be expressed as

$$N_{\rm i} = \frac{N_{\rm H}\gamma A_{\rm e}}{T_0}\int_{T_{\rm min}}^{T_0}\left(\frac{T}{T_0}\right)^{\gamma-1} f_{\rm i}(T)dT, \qquad (4)$$

where $N_{\rm H} = n_0 h_{\rm n}\xi/\sin b$, and $A_{\rm e}$ and $f_{\rm i}(T)$ are the element abundance and ionization fraction for the ion, and $T_{\rm min} = 10^5$ K is the minimum temperature assumed (line emission and absorption below this temperature are negligible; Fig. 1).

Similarly, the emission intensity (from a single line or a continuum) is

$$I = \frac{A_{\rm e}}{4\pi}\int_0^L \Lambda(T)n_e ndL = \frac{A_e}{4\pi}\int_{T_{\rm min}}^{T_0}\Lambda(T)\frac{dEM}{dT}dT, \qquad (5)$$

where $\Lambda(T)$ is the corresponding emissivity of the hot gas. The differential EM is

$$\frac{dEM}{dT} = \frac{1.2N_{\rm H}^2\gamma}{T_0 L}\left(\frac{T}{T_0}\right)^{2\gamma-1}, \qquad (6)$$

where the factor 1.2 accounts for the helium contribution to the electron density, and $L = h_{\rm n}\xi/\sin b$, is the effective pathlength of the hot gas.

Both the emission and absorption data can be used independently to constrain the parameters N_H, T_0, γ, and the relative element abundances (e.g., Ne/O; Eqs. 4 and 5). A simultaneous fit to the emission and absorption further allows for the estimate of the L parameter (Eq. 6). We have revised our absorption line model developed in Yao & Wang (2005) and the thermal emission model *cevmkl* in XSPEC to facilitate the use

TABLE 3
SPECTRAL FITTING RESULTS

	T[a] (10^6 K)	EM (10^{-3} cm^{-6} pc)	$N_{\rm H}^b$ (10^{19} cm^{-2})	γ	$h_{\rm n}$ (kpc)	N/O[c]	Ne/O[c]	Fe/O[c]	Γ^d	norm[e]
1	2.4(2.2, 2.5)	3.5(3.1, 3.9)	···	···	···	< 2.7	2.6(1.9, 3.4)	1.5(1.1, 2.1)	1.6(1.5, 1.8)	13(12, 14)
2	1.3(0.8, 2.0)	···	2.3(1.5, 3.7)	···	···	< 2.2	1(fix)	1(fix)	···	···
3	3.6(2.9, 4.7)	···	2.3(1.4, 3.8)	0.5(0.1, 1.7)	2.8(1.0, 6.4)	< 2.1	1.7(1.3, 2.3)	0.9(0.7, 1.1)	1.6(1.4, 1.7)	12(11, 13)
4	3.5(2.9, 3.9)	···	2.0(1.4, 2.4)	0.8(0.4, 1.1)	2.6(1.1, 5.8)	< 2.1	1.7(1.3, 2.3)	0.9(0.7, 1.3)	1.6(1.4, 1.7)	11(11, 13)
5	2.8(2.1, 3.1)	3.0(2.6, 3.4)	···	···	···	< 3.3	2.0(1.2, 3.3)	1.0(0.7, 2.1)	1.6(1.4, 1.7)	13(11, 14)
6	3.0(2.6, 4.3)	···	2.0(1.4, 2.8)	0.9(0.5, 1.3)	2.1(0.6, 6.9)	< 2.1	2.2(1.7, 2.9)	1.3(1.0, 1.6)	1.6(1.5, 1.8)	12(11, 13)
7	3.5(3.0, 4.1)	···	2.0(1.7, 2.3)	0.8(0.4, 1.0)	2.8(1.4, 4.5)	< 1.2	2.0(1.5, 2.7)	0.9(0.7, 1.2)	1.7(1.3, 2.0)	11(10, 12)

NOTE. — [a] For rows 1, 2, and 5, T is gas temperature for the isothermal case, and for rest rows, it is the gas temperature at the Galactic plane T_0. [b] The equivalent hydrogen column density in the hot ISM under the assumption of the solar abundance of oxygen. [c] Element abundance ratios in units of the solar values. [d] The power-law index. [e] The normalization of the power-law component, in unit of photons s^{-1} cm^{-2} keV^{-1} sr^{-1}. The listed N/O, Γ, and *norm* are constrained from AO1 observations, and the values from SWG data are given separately in the following. The horizontal dotted symbols indicate that the constraints are not applicable in the fitting. See text for details.
Row 1: Results from fitting the emission data (§ 3.1). Values of N/O, Γ, and *norm* from SWG data are 5.9(3.7, 7.8), 1.5(1.4, 1.6), and 15.4(14.5, 16.5), respectively.
Row 2: Results from fitting the absorption data (§ 3.2).
Row 3: Results from the joint analysis of the X-ray absorption and emission data (§ 3.3). Values of N/O, Γ, and *norm* from the SWG data are 4.9(3.4, 6.6), 1.4(1.3, 1.5), and 15.2(14.4, 16.1) respectively.
Row 4: Results from joint analysis of all observations with *Chandra*, *Suzaku*, and *FUSE* (§ 3.4).
Rows 5 and 6: The same as rows 1 and 4, respectively, except for allowing the EM of the LHB plus the SWCX component to vary from 0 to 0.00113 cm^{-6} pc (§ 4.1).
Row 7: Results of using a broken-PL to approach the extragalactic emission (§ 4.2). The Γ value listed here is for $E < 1.0$ keV, and for $E \geq 1.0$ keV Γ = 1.4(1.3, 1.5). For SWG data, N/O = 3.4(1.5, 5.7) and *norm* = 15.2(14.7, 16.2).

of the ionic column density N_i and the EM as a power law function of T (Eqs. 4, 5, and 6; Yao & Wang 2007).

These revised models are then used to jointly fit the absorption and emission data. For the absorption data, the fit includes not only the significantly detected O VII and Ne IX Kα lines, but also the key non-detections of the O VII Kβ, Fe XVII L, and Kα transitions of O VIII, Ne X, N VII, and N VI at 18.626, 15.010, 18.967, 12.134, 24.779, and 28.787 Å, respectively, which provide useful constraints on the physical and chemical properties of the absorbing gas. The revised *cevmkl* model is used to fit the Galactic disk component of the emission spectra (vmekal$_{\rm disk}$ in § 3.1). The abundance ratios of N/O, Ne/O, and Fe/O, which are linked together between the absorption and emission models, are allowed to vary in our fit. This joint fit is satisfactory; the directly constrained model parameters are reported in the third row of Table 3. We then infer the temperature scale height as $h_T = 1.4(0.2, 5.2)$ kpc and the gas density at the Galactic plane as $n_0 = 1.4(0.3, 3.4) \times 10^{-3}$ cm^{-3}. The confidence contours of h_n, T_0, and N_H vs. γ are plotted in Figure 5.

3.4. *Comparison with the O VI λ1031.96 absorption line*

From the non-isothermal Galactic disk model constrained with the X-ray emission and absorption data, we estimate the total O VI contained in the diffuse hot gas as $N_{\rm OVI} \sim 3.4 \times 10^{14}$ cm^{-2}, which is consistent with that inferred from the observed O VI λ1031.96 line absorption (Fig. 6; see also Wang et al. 2005; § 2.2). Including the O VI line in our joint analysis tightens the constraints on the model parameters (the forth row of Table 3), especially on the temperature distribution.

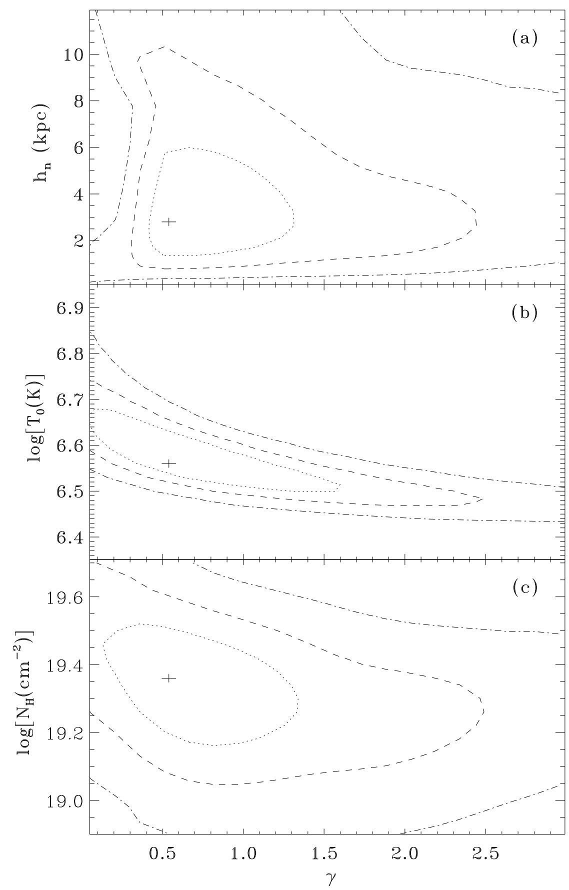

FIG. 5.— The 68%, 90%, and 99% confidence contours of $h_{\rm n}$, T_0, and $N_{\rm H}$ vs. γ, obtained in a joint fit to the X-ray absorption and emission data (§ 3.3).

4. DISCUSSION

We have presented the high quality *Suzaku* emission observations of the diffuse hot gas toward two off-fields of the LMC X–3 sight line. In particular, the O VII and O VIII emission lines are clearly resolved. Modeling these emission spectra yields a gas temperature that is about two times higher than that inferred from the high resolution absorption data. We find that our non-isothermal thick Galactic gaseous disk model can account for this discrepancy as well as the far-UV O VI absorption data. A joint fit to these data indicates that both the X-ray absorption and emission and the far-UV absorption are consistent with being produced from hot gas in a region of several kpc around the Galactic plane. In the following, we first discuss how our results are potentially affected by caveats in our data analysis, and then discuss the implications of our results on the origin and cooling of the O VII- and O VI-bearing gases.

4.1. *Uncertainty of the LHB and the SWCX*

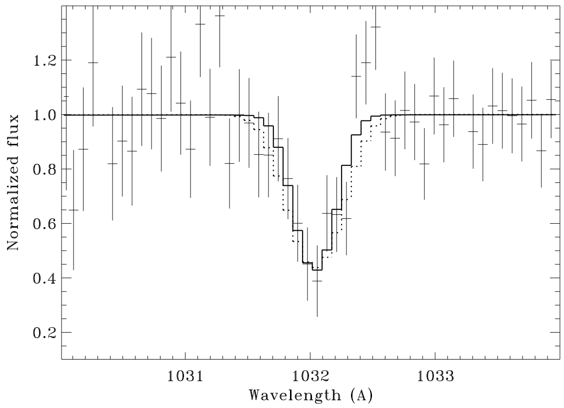

FIG. 6.— O VI absorption line at 1031.96 Å observed with *FUSE* and the best-fit model (*solid histogram*). The dotted histogram represents the predicted absorption from the X-ray data constrained non-isothermal disk model.

The biggest uncertainty in modeling the SXB emission is the estimate of the contributions from the LHB and SWCX. Our understanding for both components is still very poor because it is very hard to decompose their contributions. The SWCX emission could in principle be estimated by tracing the solar wind flux and the neutral atoms in the Earth's atmosphere and in the local ISM (e.g., Lallement et al. 2004). However, such an estimation is model dependent. For instance, for the line of sight with Galactic coordinates (l,b) = $(278.65°,-45.30°)$ observed on 2003 March 3, the O VII emission is estimated to be 0.83 and 3.7 LU by Koutroumpa et al. (2007) and by Henley & Shelton (2008), respectively. Recent comparisons of the observed X-ray emission with models for the SWCX suggest that the foreground emission in the shadowing experiments can be mainly attributed to the SWCX and that the LHB emission is negligible (Koutroumpa et al. 2007; Rocks et al. 2007; but also see Shelton 2008). The total O VII intensity of the SXB toward a high Galactic latitude sight line $(l,b = 272°,-58°)$ is 2.7(2.0, 3.4) LU (1σ range), obtained from a recent *Suzaku* observation (Mitsuda et al. 2006). If emission from both the LHB and the SWCX is isotropic and independent of Galactic latitude, this value can be regarded as the upper limit of the combined contribution of these two components.

Our results are not qualitatively affected by above discussed uncertainties. To be more quantitative in assessing the effect, we allow EM of the LHB plus SWCX component to vary from 0 to 0.0113 cm^{-6} pc (§ 3.1), representing two extreme cases. The low boundary corresponds *zero* emission of the LHB and the SWCX components, whereas the high boundary corresponds to the 3σ upper limit of the observed O VII intensity (i.e., 4.8 LU) toward the high Galactic latitude sight line. We then re-perform our spectral analysis described in §§ 3.1 and 3.4. We find that new constrained gas temperature in modeling the emission data alone under the isothermal assumption is still about two times higher than that constrained from the absorption data (refer to the first and the fifth rows in Table 3), which still necessitates the non-isothermal model developed in § 3.3. The new results constrained in the joint analysis are also consistent with the old values, except for with a slightly broader uncertain range (refer to the forth and the sixth rows in Table 3).

4.2. *Uncertainty of the extragalactic power-law component*

In modeling the emission spectra, we used a simple PL function to approximate the extragalactic contribution (§ 3.1). Recent *Chandra* and *XMM-Newton* deep surveys for the cosmic X-ray background have resolved $\gtrsim$80% of the background emission at 1-8 keV into extragalactic discrete sources (e.g., Hickox & Makevitch 2006). Optically bright sources tend to be spectrally hard while faint sources tend to be spectrally soft (e.g., Mushotzky et al. 2000). To examine the goodness of our approximation, we replace the simple PL with a broken PL and fix the break energy at 1 keV to model the extragalactic component in our joint analysis described in § 3.3. We obtain the photon indices as 1.7(1.3, 2.0) and 1.4(1.3, 1.5) below and above 1 keV, respectively, and find that the parameters of the Galactic hot gas are barely affected (the seventh row of Table 3).

4.3. *Effect of resonant scattering of the O VII line emission*

In this work, we have assumed the emitting/absorbing gas to be optically thin, i.e., we have neglected the resonant scattering effect of the hot gas. To qualitatively assess the validity of our assumption, we assume the hot gas density to be uniform for easy of analysis. The observed O VII emission line consists of unresolved triplet transitions, resonance, forbidden, and intercombination lines at 21.60 Å, 22.10 Å, and 21.80 Å, respectively. Since the oscillation strength is essentially zero for the latter two transitions, we consider the "scattering" only for the resonant line. The absorbed resonant photons should be re-emitted isotropically; half of these re-emitted photons are expected to favor the observing direction. Taking all these into account, we obtain the observed line intensity as

$$I = (1-f)I_0 + 0.5 f I_0 \left(1 + \frac{1-e^{-\tau}}{\tau}\right), \quad (7)$$

where τ is the (max) absorption optical depth at center wavelength of the resonant transition, and I_0 is the "intrinsic" (without the scattering) line intensity. Here, f is the resonant transition fraction of the O VII triple, which is a function of gas temperature. Taking the (max) temperature at the Galactic plane $T_0 \sim 3\times10^6$ K (Table 3), which favors more to the resonant transition and gives f = 0.65, we get $I \gtrsim 0.675 I_0$ for any value of τ. This indicates that the observed intensity should not be different from the intrinsic value by a factor larger than 1.5. In reality, the "background" gas cloud also scatters the photons emitted by the "foreground" cloud to the observing direction. If this effect is further considered, the difference should largely disappear. Therefore we conclude that the resonance scattering should not significantly affect our results, although a more detailed modeling needs to be performed to account for a more realistic geometry of the hot gas distribution.

4.4. *Origin of the O VII-bearing gas in general*

Our analysis indicates that the gas responsible for the observed X-ray absorption/emission along the LMC X–3 sight line has a pathlength about a few kpc and is consistent with the Galactic disk in origin. This result has important implications for understanding the structure and origin of hot gas around our Galaxy. As described in § 1, high ionization X-ray absorption lines with zero velocity shift have been observed along many extragalactic sight lines, and the O VII emission lines are also detected at various high Galactic latitudes. Several scenarios have been proposed for the origin of the emitting/absorbing gas, including the intergalactic medium (IGM) of the Local Group, the large-scale Galactic halo, and the thick Galactic gaseous disk (see Yao & Wang [2007] for a review). These scenarios cannot be distinguished kinematically because of the limited spectral resolution of current X-ray instruments. So currently the most direct information about the location of the gas comes from differential analysis of the X-ray absorption lines toward sources at different distances. Wang et al. (2005) find that the O VII absorption along the sight line toward LMC X–3, at a distance of ~ 50 kpc, is comparable to those observed toward AGN sight lines. Therefore, if the LMC X–3 sight line is representative, one can then conclude that the bulk of the X-ray absorption around the Galaxy is within ~ 50 kpc. A similar conclusion has been reached based on the estimate of the total baryonic matter contained in the O VII-bearing gas, and on the angular distribution of the O VII absorption (Fang et al. 2006; Bregman & Lloyd-Davies 2007). A comparison of a Galactic sight line (4U 1957+11) with two extragalactic sight lines toward LMC X–3 and Mrk 421 further indicates that there is no significant O VII absorption in the extended Galactic halo beyond a few kpc (Yao et al. 2008), which is consistent with the conclusion drawn in this work.

The O VII emission from the hot gas beyond LMC X–3 is not expected to be important either. Yao et al. (2008) obtained a 95% upper limit to the O VII absorption beyond LMC X–3 as $N_{\rm OVII} < 3.7 \times 10^{15}$ cm^{-2}. Assuming this much of O VII uniformly distributed in a region with an extension scale of l, we calculate its emission as $I_{\rm OVII} < 0.025/(A_{\rm O0.1} l_{\rm 100kpc})$ LU for the entire temperature range from 10^5 to 10^7 K, where $A_{\rm O0.1}$ is the oxygen abundance in unit of 10% solar value and $l_{\rm 100kpc}$ is in unit of 100 kpc. In contrast, the inferred the O VII intensity of the Galactic disk diffuse gas is 5.0 LU (§ 3.1; Table 2).

We have shown that the X-ray emission and absorption as well as the far-UV O VI absorption along the sight line toward LMC X–3 can be explained by the presence of a thick Galactic hot gaseous disk. A similar explanation holds for the sight line toward Mrk 421, for which another joint X-ray absorption/emission and UV-absorption has been carried out (the X-ray emission is, however, mostly based on the RASS broadband measurements; Yao & Wang 2007). The characteristic scale height of the disk is also consistent with the Ne IX column density distribution in the Galaxy (Yao & Wang 2005). The gas in the disk is shown to have a normal metal abundances (Wang et al. 2005; Yao & Wang 2006) and is clearly due to the heating by mechanical energy feedback from stars in the Galaxy (e.g., Ferrière [1998]). Such an interpretation is also supported by the X-ray emission observations of nearby disk galaxies like our own. The diffuse X-ray emission has been routinely observed in many late-type normal star-forming spirals and is confined to a region around galaxies with vertical extent no more than a few kpc (e.g., Wang et al. 2001, 2003; Tüllmann et al. 2006a, 2006b). Both the intensity and the spatial extent appear to be scaled with galactic star formation rate (e.g., Tüllmann et al. 2006b). Therefore, we conclude that the X-ray emitting/absorbing and O VI-absorbing gas, as studied in this paper, arises primarily from the stellar feedback in the Galactic disk.

4.5. *Location of the O VI-bearing gas*

Before discussing the O VI-bearing gas location, let us look at the O VI emission properties first. In § 3.4 we have shown that the observed O VI absorption can be predicted from the X-ray-data-constrained non-isothermal gas model and have then used the O VI λ1031.96 absorption line to further constrain our spectral model. With the fitted model parameters, we can estimate the intrinsic O VI emission intensity of the diffuse hot gas toward LMC X–3, and then compare it with observations. The best-fit model gives 186 LU in total for the O VI doublet $\lambda\lambda$1032 and 1038. Taking all the 90% boundaries that favor more O VI emission, we obtain a firm upper limit of 1612 LU.

There is no direct measurement of the O VI emission within 1° of the LMC X–3 sight line. Within $\sim 5^\circ$, some observations show measurable O VI λ1032 emission as $2.1-5.7 \times 10^3$ LU, while other observations only yield upper limit even with longer exposures (Otte & Dixon 2006; Dixon et al. 2006; Dixon & Sankrit 2008). Since the O VI emission could vary by a factor of > 2.3 at an angular scale as small as $25'$ (Dixon et al. 2006), it is nearly impossible to reliably estimate the O VI emission toward LMC X–3 sight line based on the few existing nearby samples. However, if there were a measurable O VI emission toward the LMC X–3 sight line (but see below), it must be in order of several thousand LU, as typically observed at high galactic latitudes, which is significantly larger than that predicted in the O VII-bearing gas and therefore unlikely arises from the diffuse hot gas.

Where is the O VI-bearing gas then? To answer this question, it is important to compare the spatial distributions of the O VI absorption and emission. In this work, we find that most of the O VI absorption can arise from the diffuse gas along a vertical scale of $\sim$3 kpc around the Galactic plane. Figure 7 shows the density and column density distributions of O VI and O VII as a function of the vertical distance, predicted from our constrained non-isothermal disk model. While compared to O VII, O VI is distributed in a relative narrow region, which is mainly due to the sensitive dependence of O VI population on temperature (Fig. 1), about 80% of the O VI column still spreads over as large as 1 (from 2.7 to 3.7) kpc. Observationally, O VI absorption has been detected toward essentially all sight lines, and the characteristic scale height of the O VI column densities is similar to that constrained in this work (e.g., Savage et al. 2003). It has been suggested that O VI could largely arise at interfaces between hot and cool interstellar media. However, for Mrk 421 sight line, Savage et al. (2005) counted the number of cool gas velocity components and found that the interfaces can only account for at most 50% of O VI absorption, leaving a bulk of the O VI to other origins. In contrast, the O VI emission is measured toward only $\sim 30\%$ of the surveyed sky (Otte & Dixon 2006; Dixon & Sankrit 2008). These results clearly indicate that the "commonly" observed O VI-absorbing gas in kpc scale is not primarily responsible for the detected O VI emission. We propose that the low temperature regime of the kpc-scale diffuse gas could contain a significant or even dominant fraction of the observed O VI absorption, as indicated in this work, and that the conductive interfaces between hot and cool gases, though could be another reservoir of O VI ion, is mainly responsible for the observed O VI emission. This picture not only explains the spatial distribution of the O VI absorption, but also naturally explains the sight line to sight line O VI variation in both absorption and emission. For LMC X–3 sight line in particular, since all the observed O VI can be attributed to the diffuse gas, the O VI emission is not expected to be strong.

4.6. *Radiative energy loss rate of the hot gas*

If hot gas toward the LMC X–3 sight line represents reasonable well the hot ISM of the Galactic disk as a whole, we can then use our non-isothermal gas model to estimate the total radiative energy loss rate of the gas, and compare it to

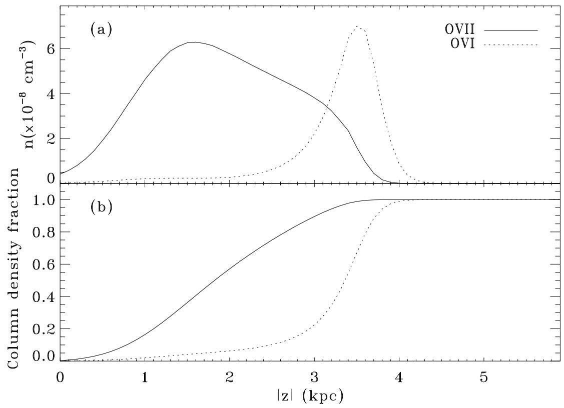

FIG. 7.— Spatial distribution of density (a) and column density (b) of O VI and O VII, predicted with our constrained non-isothermal disk model.

the expected energy input from SN explosions. It has long been observed that in the low L_x/L_B (L_B is the blue luminosity) early-type galaxies, X-ray radiative energy loss rate of the diffuse hot gas is far less than the expected SN energy input (e.g., Canizares et al. 1987; Brown & Bregman 2000). However, all the previous studies were based on imaging observations in which decomposing different emission components is a complicated task (e.g., Li et al. 2007) and could make the inferred properties of the "true" diffuse hot gas very uncertain. The LMC X–3 sight line is so far the only sight line along which the high resolution X-ray emission/absorption and far-UV absorption measurements with a minimal confusion are available, which allow us to tightly constrain the thermal and chemical properties as well as the global spatial distribution of the Galactic diffuse hot gas, as presented in this work. It is thus worthwhile reexamining the radiative power of the Galactic hot gas based on these characterizations.

The energy loss rate of the hot gas can be expressed as

$$\frac{d^2U}{dsdt} = 2\times\int_0^\infty 1.2n^2\Lambda(T)\,dz, \quad (8)$$

where the factor 2 accounts for the two sides of the Galactic disk. With our model (Eq. 1), we can rewrite the Eq. 8 as

$$\frac{d^2U}{dtds} = 2\times\int_{T_{min}}^{T_0} 1.2n_0^2\left(\frac{T}{T_0}\right)^{2\gamma-1}\Lambda(T)(-h_T)\,d\left(\frac{T}{T_0}\right). \quad (9)$$

Assuming the solar abundances, plugging in the best-fit n_0, T_0, γ, and h_T values (§ 3.3), and taking the emissivity $\Lambda(T)$ from the atomic database ATOMDB[7], we obtain the local surface emissivity of the hot gas as 3.1 and 16.1 $\times 10^{36}$ ergs s^{-1} kpc^{-2} in 0.1-10 and 0.01-10 keV bands, respectively. Including the additional O VI emission of $\sim$3000 LU from the interface component, the total radiative energy loss rate is $\sim 3\times10^{37}$ ergs s^{-1} kpc^{-2}.

The radiative cooling of the Galactic disk hot gas only accounts for less than 10 per cent of the expected energy input of the stellar feedback. At Sun's galactocentric radius, the SN rate is 19 and 2.6 Myr^{-1} kpc^{-2} for type II and type Ia, respectively (Ferrière 1998). If on average each type II SN progenitor releases 2×10^{50} ergs of energy before it explodes and each SN explosion releases 10^{51} ergs (Ferrière 1998; Leitherer et al. 1992), the total energy input is then 8×10^{38} ergs s^{-1} kpc^{-2}, which is about 20 times higher than our estimated gas cooling rate. The "missing" energy could be either emitted in other wavelength bands (e.g., infrared) or have been consumed in driving other Galactic activities (e.g., galaxy-size out flows).

[7] http://cxc.harvard.edu/atomdb

Obviously, such an estimation is model dependent. Shelton et al. (2007) recently concluded that $\sim$ 70% of the SN energy input could be radiated away by the Galactic hot gas. In their model, they required the observed O VI emission to be co-spatial with the O VI absorption and assumed both the O VI-bearing and the hotter O VII-bearing gas to be isobaric. This requirement results in that most of the O VI-bearing gas is confined within a region of $<$ 100 pc in size, which favors to produce about ten times more thermal emission in the energy range of 0.01-0.1 keV than our model. In contrast, we constrain our model with X-ray O VII and O VIII emission and absorption, and find that the most of the O VI absorption could arise from the kpc-scale diffuse gas. In our model, because of large extent of the diffuse gas (therefore a low density), its emitting power is at most as much as that of the observed/expected O VI emission lines, which presumably arise from the interfaces between the hot and cool interstellar media (§ 4.5). The scale size of the O VII- and O VI-bearing gas derived in this work and utilized in our estimation, is consistent with that obtained in the recent O VI absorption surveys (Savage et al. 2003; Bowen et al. 2008).

4.7. *Evidence for oxygen and iron depletion?*

In our analysis, we find that, while the relative abundance of Fe/O is about the solar value, the Ne/O is about 2 times higher (Table 3). This overabundance of neon, if true, is consistent with the interpretation of about 50 per cent of oxygen and iron being depleted into dust grains. However, because this overabundance is mainly derived from the emission data in which decomposing various components is still very uncertain, the depletion interpretation therefore may not be unique. For instance, Henley & Shelton (2008) suggest that the SWCX could also produce apparent non-solar abundance ratio. Furthermore, our understanding of the chemical abundances in the solar system is still poor. For example, the oxygen value has recently been revised downward by $\sim$ 35% (Asplund et al. 2005), but this revision is still under debate (Antia & Basu 2006). The abundance pattern in the ISM is also suggested to be slightly different from that in the solar system (Wilms et al. 2000). So it is more useful to list the number density ratio of Ne/O derived in this work, which is 0.25(0.19, 0.33). We prefer to defer the interpretation of the apparent overabundance of neon until a better understanding of both the SWCX and the solar chemical abundances is reached.

5. SUMMARY

We have presented an extensive study of diffuse hot gas along the sight line toward LMC X–3, based on new *Suzaka* X-ray CCD observations of the background emission as well as high resolution X-ray and far-UV absorption data. Our main results and conclusions are summarized in the followings:

1. We have detected O VII, O VIII, and Ne IX emission lines in the *Suzaku* emission spectra. Modeling these emission data gives a characteristic temperature for the emitting gas as $2.4(2.2, 2.5)\times10^6$ K, assuming the gas to be isothermal and in the collisional ionization equilibrium. This temperature is about two times higher than that inferred from the X-ray absorption data under the same assumptions. Adopting different neon to oxygen abundance ratio in analyzing the absorption

data will not relieve this discrepancy. This inconsistency indicates the non-isothermality of the emitting/absorbing gas.

2. We find the X-ray emission/absorption data are consistent with a non-isothermal hot gas model, in which both the gas temperature and the gas density decrease exponentially with the vertical distance away from the Galactic plane. Jointly analyzing the X-ray emission and absorption data, we have constrained the scale heights and the middle plane values of the gas density and temperature as 2.8(1.0, 6.4) kpc and $1.4(0.3, 3.4)\times10^{-3}$ cm^{-3}, 1.4(0.2, 5.2) kpc and $3.6(2.9, 4.7)\times10^{6}$ K, respectively. These scale heights indicate that the bulk of O VII absorption observed in the extragalactic sources (e.g., Mrk 421) is consistent with a Galactic in origin, although additional relatively small extragalactic contribution can not be ruled out.

3. We find that the above X-ray constrained non-isothermal hot gas model can naturally explain all the observed O VI line absorption, but only accounts for less than 10 per cent of the O VI emission typically observed at high galactic latitudes. We propose that most of the O VI absorption arises from the kpc-scale diffuse gas and that the O VI emission arises chiefly from interfaces between hot and cool media.

4. The cooling of the Galactic disk hot gas described here is only responsible for less than 10 per cent of the expected total SN energy input. The bulk of the SN energy is thus "missing" and may be radiated away in other wavelength bands or may have been driven into a large-scale low-density Galactic halo or into the intergalactic space.

We gratefully acknowledge extensive conversations with Blair Savage on the resonant scattering issue and conversations with Robin Shelton on the emission from the Local Hot bubble and the SWCX. We are also grateful to Claude Canizares for useful discussions and the anonymous referee for comments, which helped to clarify our presentation. This work is supported by NASA through the Smithsonian Astrophysical Observatory contract SV3-73016 to MIT for support of the Chandra X-Ray Center under contract NAS 08-03060 and NASA/GSFC grant NNX07AB06G to University of Massachusetts.

REFERENCES

Anders, E., & Grevesse, N. 1989, Geochim. Cosmochim. Acta, 53, 197
Antia, H. M., & Basu, S. 2006, ApJ, 644, 1292
Asplund, M., Grevesse, N., & Sauval, J., 2005, ASPC, 336, 25
Birnboim, Y, & Dekel, A. 2003, MNRAS, 345, 349
Brown, B., & Bregman, J. N. 2000, ApJ, 539, 592
Bowen, D. V., et al. 2008, ApJS, 176, 59
Bregman, J. N., & Lloyd-Davies, E. J. 2007, ApJ, 669, 990
Burrows, D. N., & Mendenhall, J. A. 1991, Nature, 351, 629
Canizares, C. R., Fabbiano, G., & Trinchieri, G. 1987, ApJ, 312, 503
Dixon, W. V. D., Sankrit, R., & Otte, B. 2006, ApJ, 647, 328
Dixon, W. V. D., & Sankrit, R. 2008, ApJ, in press, astro-ph/0807.1237
Fang, T., et al. 2006, ApJ, 644, 174
Ferrière, K. 1998, ApJ, 497, 759
Fujimoto,R. et al. 2007, PASJ, 59, S133
Futamoto, K., et al. 2004, 605, 793
Galeazzi, M., et al. 2007, ApJ, 658, 1081
Henley, D. B., Shelton, R. L., & Kuntz, K. D. 2007, ApJ, 661, 304
Henley, D. B., & Shelton, R. L. 2008, ApJ, 676, 335
Hickox, R. C., & Markevitch, M. 2006, ApJ, 645, 95
Hutchings, J. B., et al. 2003, ApJ, 126, 2368
Ishisaki, K. et al. 2007, PASJ, 59, S53
Jenkins, E. B. 1978, ApJ, 219, 845
Juett, A., et al. 2006, ApJ, 648, 1066
Koutroumpa, D., et al. 2007, A&A, 475, 901
Koyama et al. 2007, PASJ, 59, S23
Kuntz, K. D., & Snowden, S. L. 2001, ApJ, 554, 684
Lallement, R., et al. 2004, A&A, 426, 875
Leitherer, C., Bobert, C., & Drissen, L 1992, ApJ, 401, 596
Li, Z., Wang, Q. D., & Hameed, S. 2007, MNRAS, 376, 960
McCammon, D., et al. 2002, ApJ, 576, 188
Mitsuda, K. et al. 2006, AAS, 208, 3910
Mitsuda, K. et al. 2007, PASJ, 59, S1
Mitsuda, K. et al. 2008, Prog. of Theor. Phys. Suppl. , 169, 79
Mushotzky, R. F., et al. 2000, Nature, 404, 459
Otte, B., & Dixon, W. V. D 2006, ApJ, 647, 312
Page, M. J., et al. 2003, MNRAS, 345, 639
Park, S., et al. 1997, ApJ, 476, L77
Rocks, L. E., McCammon, D., Bauer, M., Fujimoto, R., & Mitsuda, K. 2007, AAS, 20925418
Savage, B. D., et al. 2003, ApJS, 146, 125
Savage, B. D., et al. 2005, ApJ, 619, 863
Savage, B. D., & Lehener, N. 2006, ApJS, 162, 134
Sembach, K., & B. D. Savage, 1992, ApJS, 83, 147
Shelton, R. L., et al. 2001, ApJ, 560, 730
Shelton, R. L., Shallmen, S. M., & Jenkins, E. B. 2007, ApJ, 659, 365
Shelton, R. L. 2008, SSRv, tmp, 69
Shull, J. M., & Slavin, J. D. 1994, ApJ, 427, 784
Smith, R. K., et al. 2007, PASJ, 59, S141
Snowden, S. L., et al. 1997, ApJ, 485, 125
Sutherland, R. S., & Dopita, M. A. 1993, ApJS, 88, 253
Tawa et al. 2008, PASJ, 60, S11
Tüllmann, R., et al. 2006a, A&A, 448, 43
Tüllmann, R., et al. 2006b, A&A, 457, 779
Wang, Q. D., et al. 2001, ApJ, 555, L99
Wang, Q. D., et al. 2003, ApJ, 598, 969
Wang, Q. D., et al. 2005, ApJ, 635, 386
Wilms, J., Allen, A., & McCray, R. 2000, ApJ, 542, 914
Yao, Y., & Wang, Q. D., 2005, ApJ, 624, 751
Yao, Y., & Wang, Q. D., 2006, ApJ, 641, 930
Yao, Y., & Wang, Q. D., 2007, ApJ, 658, 1088
Yao, Y., et al. 2008, ApJ, 672, L21